VACUUM ULTRAVIOLET SPECTROSCOPY AT TEXTOR

W. BIEL* and TEXTOR TEAM *Institut für Plasmaphysik, Forschungszentrum Jülich GmbH*
EURATOM Association, Trilateral Euregio Cluster, D-52425 Jülich, Germany

Received April 29, 2004
Accepted for Publication June 18, 2004

Spectroscopy in fusion experiments is an important tool to identify impurities in the plasma and to analyze their properties based on the measurement of their characteristic line radiation. For the temperature range typical in fusion plasmas, the dominant part of each impurity in the plasma is highly ionized, and its most intense spectral lines radiate in the vacuum ultraviolet (VUV) wavelength range (10 to 200 nm). The VUV overview spectrometers installed at TEXTOR working at moderate resolution allow one to identify intrinsic plasma impurities such as B (Z = 5), C (Z = 6), Fe (Z = 26), and Cu (Z = 29) as well as seeded impurities such as Ne (Z = 10) and Ar (Z = 18) and to derive information on their relative densities in the plasma. Optimizing these spectrometers for high time resolution provides a tool to analyze transient phenomena like impurity transport processes. In combination with impurity transport modeling and atomic data, the radial distribution of the radial diffusion coefficient is determined from the experimental data. For the case of ohmic discharges, the effective radial diffusion coefficient is found to be anomalously enhanced by more than one order of magnitude as compared to neoclassical predictions.

KEYWORDS: *VUV spectroscopy, plasma impurities, impurity transport*

I. THE ROLE OF VUV SPECTROSCOPY IN FUSION PLASMAS

The performance of magnetically confined fusion plasmas is strongly related to the content and transport of plasma impurities, which include all elements in the plasma apart from the hydrogen fuel. Impurities are either released to the plasma via the plasma-wall contact[1,2] or produced by the fusion reaction (helium) or added artificially to modify the plasma radiation properties.[3–5] The most fundamental experimental access to identify impurity species is the measurement of their characteristic line radiation by spectroscopy.[6,7] Under the plasma conditions typical for magnetic fusion experiments, the strongest spectral lines of most of the relevant impurity ions are located in the vacuum ultraviolet (VUV) wavelength range (10 to 200 nm), which can dominate the total radiation power losses of the plasma. It is therefore a fundamental task for VUV spectroscopy in fusion plasmas to characterize the impurity content in the plasma and in particular to monitor changes in the relative abundancies of the important impurity species.

In order to study the radial transport of plasma impurities, transient experiments are frequently performed where a small trace of gas or metal is injected into the plasma, and the time evolution of spectral lines from different ionization stages of these test species is measured.[8–12] During the transport of injected impurities from the cold plasma edge toward the hot plasma center, they are successively ionized multiple times, so that the occurrence of spectral lines from higher ionization stages is delayed with respect to lower stages. The measured time evolution of spectral lines from many different ionization stages is analyzed using transport modeling, yielding the radial transport properties of the impurities in the plasma. The achievable accuracy of such experiments depends on the simultaneous measurement of many spectral lines from different ionization stages with high time resolution. Therefore, the VUV spectrometers at TEXTOR have been optimized for high time resolution, operating at high *etendue* to detect a large number of photons per second and using fast detectors that allow one to continuously record 1000 full spectra/s.

In this paper, we aim to present an overview of the work performed in the field of VUV spectroscopy at TEXTOR. After a description of the VUV instrumentation that is installed at TEXTOR, the possibilities for identification of impurities in the plasma are demonstrated, based on sample spectra. Finally, we describe experimental results and the numerical analysis of impurity injection experiments.

*E-mail: w.biel@fz-juelich.de

II. VUV SPECTROMETERS AT TEXTOR

Three VUV overview spectrometers with high time resolution (1 ms) have been recently installed at TEXTOR with radial sight lines near the horizontal midplane. The survey poor resolution extended domain[13,14] (SPRED) spectrometer chamber contains two complete spectrometer branches, each consisting of an entrance slit, a toroidally shaped diffraction grating illuminated under ~20 deg in near-grazing incidence geometry, and a plane open multichannel plate detector (40-mm diameter) with a fast P46 phosphor screen to convert the VUV photons to visible light. Spectrometer channel SPRED-A uses a Au-coated diffraction grating with 450 grooves per millimeter, thus covering the entire wavelength range from 10 to 110 nm with a wavelength resolution of 0.4 nm [full-width at half-maximum (FWHM)], which is mainly determined by the detector. The second spectrometer channel SPRED-B further expands the range 10 to 33 nm with 0.1-nm resolution, using a Au-coated grating with a groove density of 2105 per mm. In addition to the double-SPRED spectrometer, a near-normal-incidence spectrometer (McPherson type 234) of Seya-Namioka type[15] is installed, which monitors the wavelength range 58 to 127 nm with 0.3-nm resolution. The data of all VUV spectrometers are summarized in Table I.

In total a wavelength range of more than one order of magnitude within the VUV range is covered (see Table I) where all the first 40 elements of the periodic table have strong emission lines. In particular, the covered wavelength range comprises intense spectral lines from H-like and He-like states of low-Z impurities (from He to C) as well as strong Mg-like, Na-like (up to Zr), B-like, Be-like, and Li-like (up to Cu) spectral lines from medium-Z impurities. Thus, these spectrometers are well suited to identify the relevant impurity species in the TEXTOR plasma.

Typical particle transport times in medium-sized fusion experiments like the tokamak TEXTOR are in the range of only 5 to 30 ms. In order to analyze transient impurity injection experiments by means of VUV spectroscopy in detail, a continuous recording of spectra with high frame rate is required. To this purpose, a fast camera head has been developed that is based on a linear array (1024 pixels, each 2.5 mm high and 0.025 mm wide) and a fast switching integrator and amplifier circuit.[16] The geometrical size of the spectra is adapted to the linear array by means of a coherent fiber taper (reducing the image from a 40- to 25-mm diameter), while the light intensity of the spectra is adapted to the full charge capacity of the arrays using an external plane first-generation light amplifier with an amplification factor of 10. The data acquisition and data evaluation are based on a standard personal computer system with an analog-digital converter card, allowing for continuous measurement of spectra with an effective 10-bit dynamical range at a full spectra rate of 1000/s. All three VUV spectrometers have been equipped and successfully operated using this fast detector technique.

TABLE I

Data of the VUV Spectrometers with High Time Resolution at TEXTOR

VUV Spectrometer System	Wavelength Range (nm)	Wavelength Resolution (nm)
Type 234 spectrometer[15]	57 to 130	0.3
SPRED-A spectrometer[13]	10 to 110	0.4
SPRED-B spectrometer[14]	10 to 33	0.1

III. IMPURITY MONITORING AND IDENTIFICATION

The impurity content in the plasma strongly depends on the composition and conditioning of the plasma-facing wall components. In the case of TEXTOR, all plasma-wetted wall components are made from graphite. Several techniques were developed to beneficially modify the properties of the walls and thereby to influence the impurity content in the plasma. In the past years mainly the boronization of the walls by a glow discharge operated in a gas mixture of 10% B_2H_6 and 90% He was used, resulting in the deposition of a thin boron layer on the inner walls, which also covers in particular the carbon tiles; see Ref. 17. VUV spectroscopy serves to monitor the temporal evolution of the impurity content in the plasma following a fresh boronization by analyzing the spectra recorded in discharges operated under standard conditions (ohmic heating, plasma current $I_p = 400$ kA, mean electron density $n_e = 2 \times 10^{19}$ m^{-3}, toroidal magnetic field $B_t = 1.9$ T); see Figs. 1, 2, and 3. Immediately after the boronization (discharge #93393), the dominant impurities in the plasma are boron and helium, which remain at the walls to some extent from the boronization discharge and to a larger extent from a subsequent glow discharge cleaning operated in pure helium. Because of the gettering effect of the freshly boronized walls, the oxygen content in the plasma is largely reduced as compared to the case of standard discharge #93552, which was performed ~550 s of total plasma operation later than #93393. The accumulated plasma operation time causes an aging of the status of the wall conditioning by erosion processes, which is clearly visible in a reduction of the boron line intensities and an increase of the carbon line intensities with time; see Fig. 2. The quantitative analysis is performed by impurity modeling using the STRAHL code,[18] which solves the system of continuity equations for the ionization stages of the impurities and

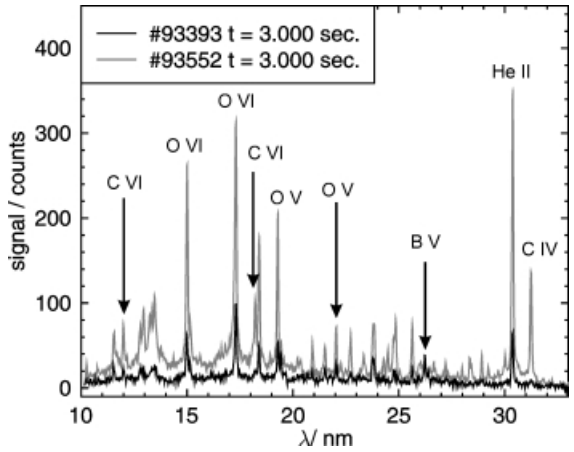

Fig. 1. VUV spectra (SPRED-B) from TEXTOR standard discharges recorded after fresh wall conditioning by boronization (#93393) and ~550 s of plasma operation later (#93552).

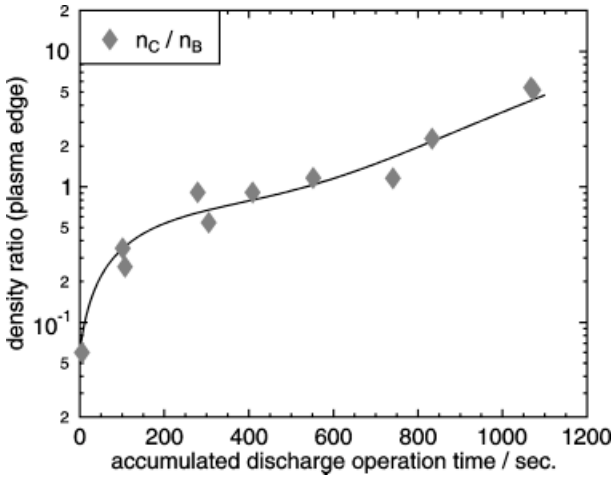

Fig. 3. Temporal development of the density ratio n_C/n_B after a fresh boronization, performed before discharge #93393.

calculates the line intensities of spectral lines. Radial profiles of the time-averaged profiles of n_e and T_e as measured by interferometry, electron cyclotron emission, Thomson scattering, and helium beam spectroscopy are used as input parameters, while the relevant atomic processes such as ionization, recombination, line excitation, and charge exchange between argon ions and the hydrogen neutral particle background are described using data from the Atomic Data and Analysis Structure database.[19] The hydrogen neutral particle density profile $n_H(r)$ is taken from a self-consistent RITM code modeling of the discharges.[20] From the numerical results we conclude that both the B III line at $\lambda = 67.7$ nm and the C III line at $\lambda = 97.7$ nm have their maximum emissivity at the same radial position of $r = 46$ cm, which facilitates to derive the impurity density ratio n_C/n_B from the measured line intensity ratio. For the case of equal absolute densities of carbon and boron, the line intensity ratio predicted from the STRAHL modeling amounts $I_{CIII,97.7nm}/I_{BIII,67.7nm} \approx 6.4$. In the further analysis of the experimental data, we take into account the relative intensity calibration of the SPRED-A spectrometer, which was obtained by measuring spectra from a secondary standard laboratory discharge with tabulated line intensities,[21] yielding $\eta_{67.7nm}/\eta_{97.7nm} \approx 2.8$. In Fig. 3 the resulting density ratio n_C/n_B is displayed for the same sequence of standard discharges as in Fig. 2. We conclude that after a fresh boronization the boron content in standard ohmic discharges is more than one order of magnitude larger than the carbon content. After typically ~500 s of plasma operation with mainly ohmically heated discharges, the same level of densities is obtained for carbon and boron. Continuing the plasma operation further, the boron layer at the plasma-wetted surfaces degrades continuously, while the relative carbon content in the plasma becomes much larger than the boron content. In the case of discharge operation with strong auxiliary heating, the observed degradation of the boronization status occurs even faster than in the case of pure ohmic heating. For a detailed treatment of the erosion, transport, and redeposition processes involved in the aging of the boronization status, we refer to Refs. 17 and 22 and the references given therein.

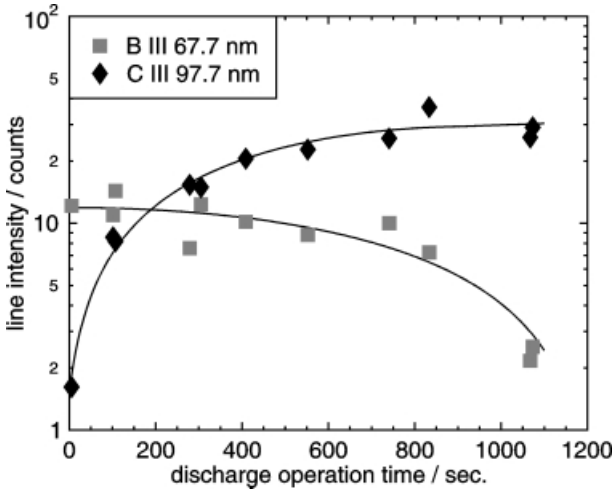

Fig. 2. Temporal evolution of line intensities from boron and carbon after a fresh boronization, performed before discharge #93393.

At TEXTOR a plasma state with improved confinement can be obtained by injecting neon into discharges with high density and strong auxiliary heating; see Ref. 23 and the references given therein. In these discharges a

feedback loop is used to keep the neon radiation level constant by controlling the neon gas inlet using the measured VUV line intensity of the Ne VIII line at $\lambda = 77.04$ nm. In Fig. 4, a typical spectrum from a radiatively improved (RI)-mode discharge phase is shown, together with a spectrum recorded just prior to the start of the neon gas injection. The VUV spectra of RI-mode discharges are completely dominated by line radiation from neon, where the most intense transitions are the Ne VII line at $\lambda = 46.52$ nm and the Ne VIII line doublet at $\lambda = 77.04$ nm and $\lambda = 78.03$ nm. Based on a STRAHL code simulation, the measured intensity ratio between the Ne VI transition at $\lambda = 40.19$ nm and the C IV transition at $\lambda = 38.41$ nm can be utilized to determine the density ratio between carbon and neon near the plasma edge region ($r \approx 44$ cm), yielding $n_{Ne}/n_C \approx 0.4$ for this discharge.

During the discharge operation one occasionally observes unexpected impurity events where elements other than the low-Z elements are released to the plasma, followed by the occurrence of the respective additional spectral lines. Either these events may be caused by an unwanted plasma-wall contact (e.g., by arcing) at those remote wall areas that are not covered by graphite, or they may be simply due to dust particles falling into the plasma. An example is shown in Fig. 5, where two different metal impurity events were detected in the course of TEXTOR discharge #92741. In the first event at $t =$ 1.8 s, the dominant elements are Ni, Cr, and Fe, which can clearly be identified based on their Mg-like, Na-like, Be-like, and Li-like resonance lines. The relative intensities observed in the spectrum are in agreement with the composition of the INCONEL® 625 alloy, from which major parts of the inner vessel of TEXTOR are constructed. The time evolution of the spectral lines of this event shows a fast increase within ~10 ms, followed by an exponential decay with decay times in the range of

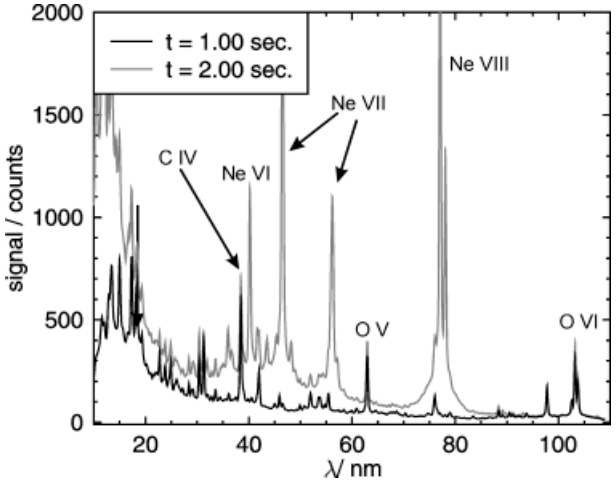

Fig. 4. VUV spectra (SPRED-A) from an RI-mode discharge (#94376).

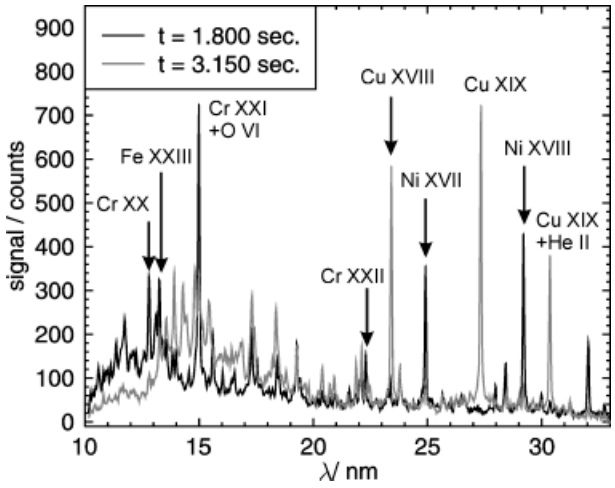

Fig. 5. VUV spectra (SPRED-B) from metal events during an ohmically heated TEXTOR discharge (#92741).

50 ms, which can be interpreted as the typical impurity confinement time in this discharge. The absolute intensities of the spectral lines observed are in agreement with a total number on the order of 10^{17} particles released to the plasma, which refers to a maximum metal concentration on the order of 0.1% in the plasma. In the second event the Mg-like and Na-like resonance lines from copper are detected with intensities and concentrations comparable to the first event.

IV. IMPURITY TRANSPORT EXPERIMENTS

In order to study the radial transport of impurities, short argon puffs (duration 2 ms FWHM) were injected into the flattop phase of a series of discharges, and the time evolution of spectral lines from argon was monitored.[12] Figure 6 shows sample spectra recorded a few milliseconds after the short argon gas puff (start of pulse at $t = 3.700$ s) had been applied into an ohmically heated discharge. Argon lines from Al-like, Mg-like, Na-like, Be-like, and Li-like ions can be clearly identified in the VUV spectra. In the plasma center, the Ar XVI and Ar XVII signals at $\lambda = 0.4$ nm are collected by means of a high-resolution X-ray spectrometer[24] installed in the horizontal midplane, while soft X-ray (SXR) cameras equipped with 100-μm Be foils monitor the central SXR radiation at different sight lines. All spectroscopic signals are recorded with high time resolution ($\leq$1 ms). In Fig. 7 normalized line intensities are displayed for discharge conditions with mean electron density $\bar{n}_e = 2.0 \times 10^{13}$ cm^{-3} and ohmic heating at a plasma current of 350 kA. All measured line intensities show a fast increase followed by a slower decay phase. The increase phase of the signals from the higher ionization stages is delayed with respect to the lower stages by typically only 5 to

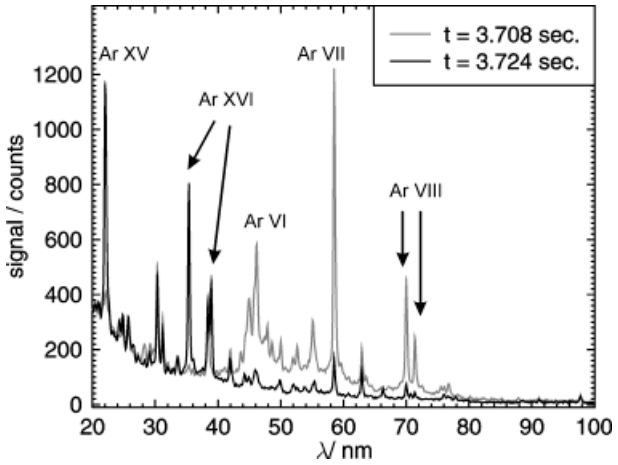

Fig. 6. VUV spectra (SPRED-A) from an argon puffing experiment ($t = 3.700$ s) during an ohmically heated TEXTOR discharge (#88711).

15 ms, showing that the bulk of the argon ions moves quite fast from the plasma edge toward the plasma center. The slow decay phase of all argon signals is determined by a combination of radial transport and recycling processes at the walls.

The quantitative analysis of the experimental results is performed by simulating the gas puff experiments using the predictive impurity transport code[18] STRAHL. In these calculations we take into account the radial transport contributions by neoclassical diffusion D_{neocl} and radial drift velocity v_{neocl} as well as the radial profile of the anomalous diffusion coefficient D_{an}, which is varied iteratively until we find agreement between the time evolution of the measured and the calculated spectroscopic signals. As the technique described here is not sufficiently sensitive for determining the magnitude of the anomalous pinch velocity v_{an}, all results presented below refer to simulations where the anomalous radial drift velocity is neglected ($v_{an} = 0$). The resulting values for the effective anomalous diffusivity are therefore labeled as $D_{an,eff}$.

The analysis is based on the normalized time traces of the spectral lines from Ar VIII (77.0 nm), Ar X (17.1 nm), Ar XII (15.4 nm), Ar XIV (18.8 nm), Ar XV (22.1 nm), Ar XVI (35.4 nm), and Ar XVII (0.4 nm). Radial profiles of the calculated normalized emissivities of these argon lines for the same discharge as given above are shown in Fig. 8. The emissivities of the measured VUV lines cover the radial region $r = 15 \ldots 45$ cm in the form of nested shells, while the emissivity of the X-ray radiation from Ar XVII (0.4 nm) is restricted to the plasma center ($r = 0 \ldots 15$ cm). Because of radial transport effects, all emissivity shells are significantly broadened and shifted toward the plasma center as compared to the predictions from a corona model; see Fig. 9.

The dense coverage of the radial region with emissivity shells allows one to derive the detailed radial profiles of $D_{an,eff}(r)$ from the STRAHL modeling; see Fig. 10. For the plasma conditions investigated here, we obtain values of $D_{core} \approx 0.2 \ldots 0.5$ m^2/s for the plasma center, $D_{max} \approx 2 \ldots 4$ m^2/s in the radial region near half-minor radius ($r \approx 25$ cm), and a decrease of $D_{an,eff}$ toward $D_{an,eff} \approx 0.5$ m^2/s near the plasma edge. The absolute figures exceed the neoclassical values by more than one order of magnitude in both the plasma center and in the outer plasma region. The elevated level of diffusivity in the radial range near half minor radius is in rough agreement with theoretical predictions from ion temperature gradient instability[25] and from gyro-Bohm behavior.[26] A

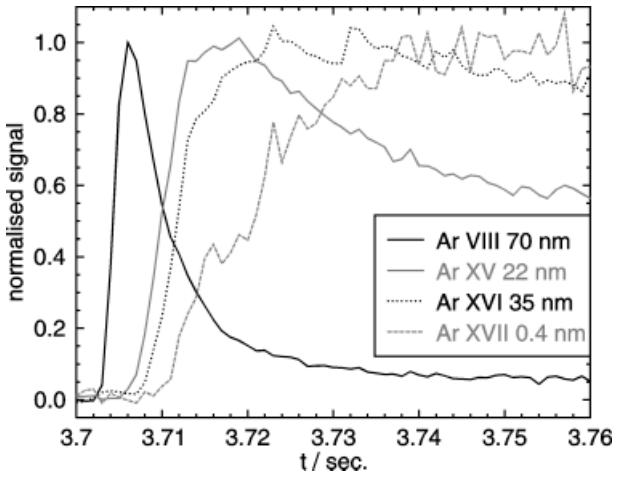

Fig. 7. Time traces of VUV and X-ray signals from an argon puffing experiment ($t = 3.700$ s) in an ohmically heated TEXTOR discharge (#88711).

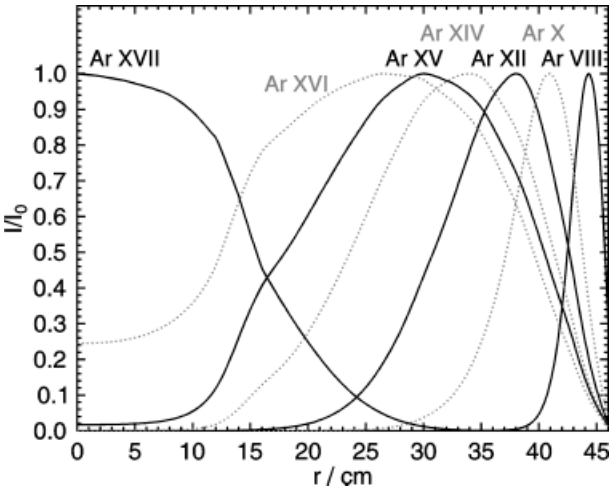

Fig. 8. Radial profiles of emissivities of spectral lines from different ionization stages (from impurity modeling of discharge #88711 using the STRAHL code).

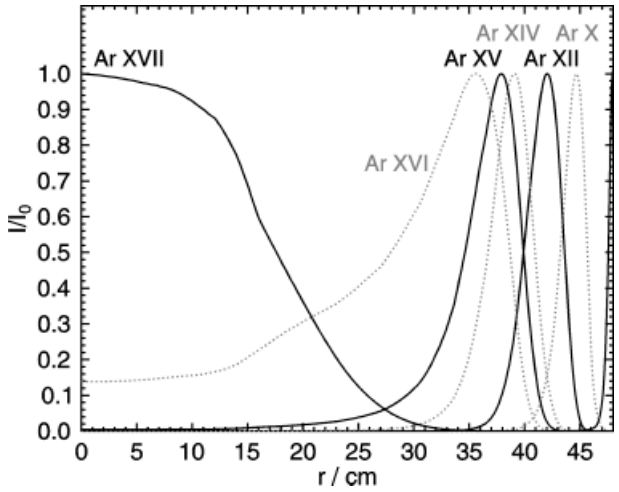

Fig. 9. Radial profiles of emissivities of spectral lines from different ionization stages as predicted from corona equilibrium, for the discharge conditions of #88711.

similar shape of the radial profile of the particle diffusivity has been found for L-mode discharges in Tore Supra.[11]

With increasing line-averaged electron density, the diffusion coefficient decreases; see Fig. 10. We find that both the central value D_{core} as well as the mean value D_{avg} show an Alcator-like scaling[27] like $D_{an,eff} \propto 1/\bar{n}_e$. Simultaneously, both the effective particle confinement time τ_P^* and the energy confinement time τ_E increase linearly with density, where the latter relation indicates that the discharges follow the linear ohmic confinement regime.[27]

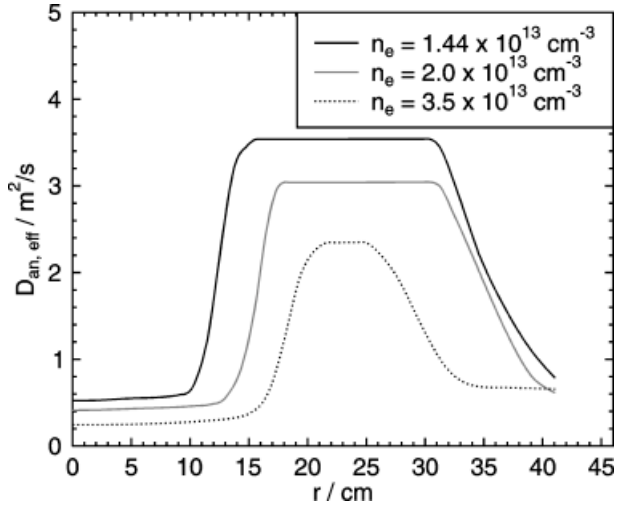

Fig. 10. Radial profiles of radial diffusion coefficient for ohmically heated TEXTOR discharges with plasma current I_P = 350 kA and toroidal magnetic field B_t = 2.25 T.

Performing similar argon puffing experiments in neutral beam–heated L-mode discharges, we observe that both the time shift between the increase phase of the different spectroscopic signals as well as the decay times of the signals after the gas puff are significantly shorter as compared to ohmically heated discharges. We conclude that the effective anomalous impurity diffusion coefficient $D_{an,eff}$ in L-mode discharges is larger than the values obtained in ohmic discharges of the same plasma density and current and that the corresponding impurity confinement times are shorter. In RI-mode discharges, similar impurity transport experiments could not be performed so far because a sufficiently high signal-to-noise ratio of the argon signals could not be obtained in the presence of the strong neon background radiation.

V. SUMMARY

VUV spectrometers with high time resolution have been installed at TEXTOR to monitor the impurity content in the plasma and to determine the radial transport properties in impurity injection experiments. More than 20 different impurity species in the range of $Z = 2 \ldots 40$ have been identified based on the most prominent resonance lines of their ions. Impurity injection experiments can be analyzed in great detail by the simultaneous measurement of spectral lines from many different ionization stages. The numerical evaluation by impurity transport modeling yields the detailed radial profile of the radial diffusion coefficient D of the impurities.

REFERENCES

1. F. WAELBROECK et al., *Plasma Phys. Control. Fusion*, **21**, 185 (1989).

2. R. NEU et al., *Plasma Phys. Control. Fusion*, **44**, 811 (2002).

3. U. SAMM et al., *Plasma Phys. Control. Fusion*, **35**, B167 (1993).

4. J. ONGENA et al., *Plasma Phys. Control. Fusion*, **38**, 279 (1996).

5. J. RAPP et al., *Plasma Phys. Control. Fusion*, **44**, 639 (2002).

6. R. C. ISLER, *Nucl. Fusion*, **24**, 1599 (1984).

7. K. H. BEHRINGER et al., *Nucl. Fusion*, **26**, 751 (1986).

8. S. A. COHEN, J. L. CECCHI, and E. S. MARMAR, *Phys. Rev. Lett*., **35**, 1507 (1975).

9. K. KRIEGER, G. FUSSMANN, and ASDEX TEAM, *Nucl. Fusion*, **30**, 2392 (1990).

10. M. A. GRAF et al., *Rev. Sci. Instrum*., **66**, 636 (1995).

11. M. MATTIOLI, C. DE MICHELIS, and A. L. PEQUET, *Nucl. Fusion*, **38**, 1629 (1998).

12. W. BIEL et al., *Proc. 28th European Physical Society Conf. Plasma Physics and Controlled Fusion*, Funchal, Madeira, Portugal, June 18–22, 2001, *European Conference Abstracts*, Vol. 25A, p. 1389 (2001).

13. R. J. FONCK et al., *Appl. Opt*., **21,** 2215 (1982).

14. B. C. STRATTON et al., *Rev. Sci. Instrum*., **57**, 2043 (1986).

15. J. A. R. SAMSON, *Techniques of Vacuum Ultraviolet Spectroscopy*, pp. 69–74, Wiley, New York (1967).

16. W. BIEL et al., *Rev. Sci. Instrum.*, **75**, 2471 (2004).

17. V. PHILIPPS, "Wall Conditioning on TEXTOR," *Fusion Sci. Technol.*, **47**, 119 (2005).

18. K. BEHRINGER, JET-R(87)08, JET Joint Undertaking (1987).

19. H. P. SUMMERS, "Atomic Data and Analysis Structure"; available on the Internet at ⟨http://adas.phys.strath.ac.uk/⟩ (2002).

20. M. Z. TOKAR, *Plasma Phys. Control. Fusion*, **36**, 1819 (1994).

21. K. DANZMANN et al., *Appl. Opt.*, **27**, 4947 (1988).

22. A. KIRSCHNER et al., "Overview of Erosion Mechanisms, Impurity Transport, and Deposition in TEXTOR and Related Modeling," *Fusion Sci. Technol.*, **47**, 146 (2005).

23. B. UNTERBERG et al., "The Radiative Improved Mode at TEXTOR: Power Exhaust and Improved Confinement at High Density," *Fusion Sci. Technol.*, **47**, 187 (2005).

24. J. WEINHEIMER et al., *Rev. Sci. Instrum.*, **72**, 2566 (2001).

25. M. Z. TOKAR et al., *Proc. 28th European Physical Society Conf. Plasma Physics and Controlled Fusion*, Funchal, Madeira, Portugal, June 18–22, 2001, *European Conference Abstracts*, Vol. 25A, p. 1049 (2001).

26. W. HORTON, *Rev. Mod. Phys.*, **71**, 735 (1999).

27. R. R. PARKER et al., *Nucl. Fusion*, **25**, 1127 (1985).